IET Power Electronics

Research Article

IET Journals
The Institution of Engineering and Technology

Improved power decoupling control strategy based on virtual synchronous generator

ISSN 1755-4535
Received on 18th August 2016
Revised 30th November 2016
Accepted on 20th December 2016
E-First on 30th January 2017
doi: 10.1049/iet-pel.2016.0608
www.ietdl.org

Bin Li[1] ✉, *Lin Zhou*[1], *Xirui Yu*[1], *Chen Zheng*[1], *Jinhong Liu*[1]

[1]*State Key Laboratory of Power Transmission Equipment & System Security and New Technology, Chongqing University, Shapingba District, Chongqing 400044, People's Republic of China*

✉ *E-mail: 20956623@qq.com*

Abstract: Virtual synchronous generator (VSG) control scheme, which can be regarded as an extension of droop control, has received much attention from researchers as the introduction of rotational inertia to inverters. This study discusses an active and reactive power decoupling technique for VSGs in microgrid, as an important aspect of VSG. The traditional power decoupling mechanism is initially analysed. Subsequently, the properties of the line impedance at different voltage degrees are compared. Results indicate that the traditional power decoupling method is unsuitable for medium- and low-voltage microgrids. Thus, an improved power decoupling method is proposed. By estimating the voltage at the point of common coupling and tracking their reference values, the output active and reactive power of inverters can perform dynamic decoupling. Furthermore, the stability of the new control structure and selection of relevant coefficients are analysed. The simulation and experimental results verify the enhanced decoupling strategy for VSGs.

1 Introduction

Distributed generation, as the main form of renewable energy power generation, plays an important role in solving the current energy crisis and environmental problems. To promote the integration of distributed power supply, some scholars have proposed microgrids [1]. A microgrid is new network structure comprising numbers of distributed generators, energy storage devices, energy conversion devices, loads and protection devices. Microgrids can flexibly implement self-control, self-protection and self-management. They can also alleviate the effect of a large number of distributed power supply accessing the grid by interacting with the grid supplement. However, compared with the synchronous generators (SGs) in a bulk power system, the power electronic inverter of a microgrid presents significant distinction on outer features, including lower capacity and output impedance. Moreover, the inverter of microgrid exhibits poor anti-disturbance capability because of the lack of system inertia. All these drawbacks will exacerbate the instability of the power system [2, 3].

To date, droop control is the most frequently used control method in microgrids. A microgrid inverter allocates active and reactive power reasonably by tracking the reference voltage signals generated by the droop controller. This method is similar to the power sharing between parallel SGs and it allows the distributed generators to realise a plug-and-play function and interconnect without communication line. However, some drawbacks are still present in its implementation process. Lacking rotational inertia, the inverter with droop control cannot provide the necessary frequency support and damping to a power system. To introduce the 'sync' mechanism of SGs to inverters, some scholars have proposed a new control named virtual synchronous generator (VSG), which enables inverters to damp power oscillations by simulating rotor motion equations and consequently enhance the stability of the system. VSG integrates the advantages of both SGs and inverters; thus, this new solution for inverters has been widely studied since its proposal [4–11].

Various optimisations for VSG have been presented according to different requirements. VSG actually uses the same power decoupling control mechanism as that of the droop control in its implementation process; this mechanism consists of an active power sharing control loop (P–f) and a reactive power sharing control loop (Q–V) [12]. The line impedance in a microgrid generally presents resistive or resistance-inductance property; Consequently, a strong coupling exists between the control of active and reactive power, and such coupling may influence the stability and dynamic performance of the power system [13]. Scholars have proposed many power decoupling strategies for droop control, which can be divided into three categories. A direct decoupling method based on relative gain array is proposed in [14, 15]. In this method, a power transformation matrix with the system impedance is constructed and a better control channel is selected by estimating the coupling relationship between power and voltage. Nevertheless, this scheme may become a voltage–active power (P–V) and frequency–reactive power (Q–f) droop strategy in a resistive line environment, which is incompatible with SGs of the existing power systems. Meanwhile, it still requires a virtual inductor to enable power decoupling. Second, virtual power decoupling method based on coordinate transformation is proposed in [12, 16, 17]. Through introducing a coordinate rotation matrix composed by the impedance angle of line, real power flows can be transformed into decoupled virtual power flows. Although the method proposed in [17] can guarantee the sharing of actual power if the distributed line impedance angles of each DG are different, this method can only avoid a large deviation from the control objective and it cannot realise complete decoupling. Third, the virtual impedance-based decoupling control is proposed in [18–21]. In this method, a virtual impedance loop is implemented by subtracting its voltage drop on the input side of the voltage loop and the impedance of system is modified to be inductive. However, a high virtual inductor is required in a resistive line environment and may aggravate the bus voltage drop. Furthermore, the value of virtual impedance is difficult to determine considering the dynamic performance and stability of the system. In [21], a virtual negative resistor is used to counteract the effect of the line resistance thus ensuring a mainly inductive system impedance. The influence of the resulting parameters on system stability is analysed. However, a correcting unit is introduced in this paper to obtain the desired decoupling effect; as a result, the complexity of the system is increased.

In this article, a new power decoupling method for VSG is proposed based on voltage at the point of common coupling (VPCC) estimator. Through tracking the reference value of VPCC, the system impedance can be modified to meet the power

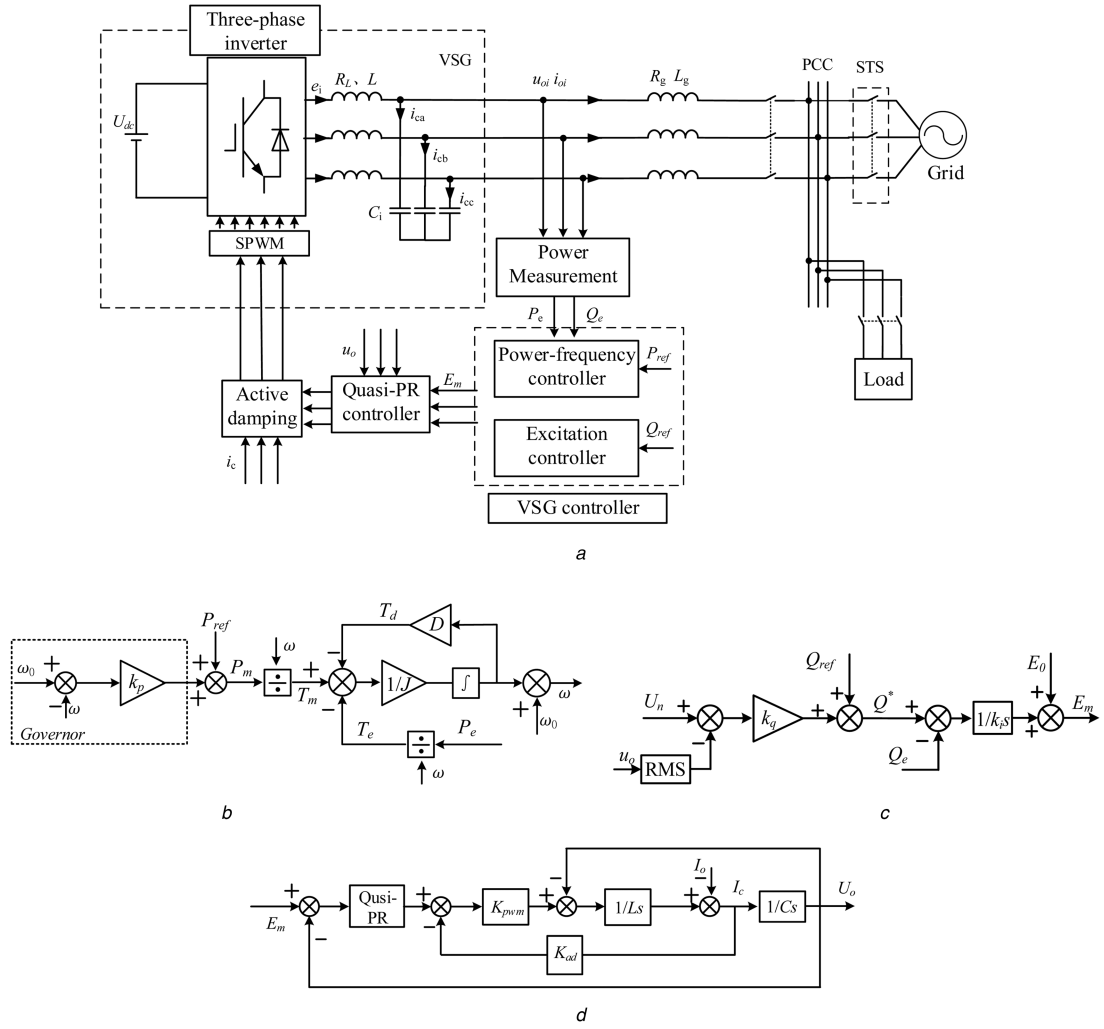

Fig. 1 *Block diagram of the VSG strategy*
(a) Main circuit, ***(b)*** Structure of the power–frequency controller, ***(c)*** Structure of the excitation controller, ***(d)*** Voltage control diagram

decoupling requirement. Different from traditional virtual impedance method, the impact of line impedance on output power can be eliminated completely rather than be weakened by applying the proposed scheme. Meanwhile, the stability of new control structure and selection of correlation coefficient are studied.

The rest of this paper is organised as follows. The VSG algorithm model is established in Section 2. Power–frequency and excitation controller are constructed by small signal analysis method, respectively. The mechanism of power coupling is studied and the conventional power decoupling method is introduced in Section 3. Subsequently, the proposed decoupling method based on VPCC estimator is fully analysed in Section 4. Finally, simulation and experimental results are obtained.

2 Control strategy of the VSG

2.1 Structure of main circuit

The topology structure of the main circuit based on the VSG control algorithm is shown in Fig. 1*a*. A direct current (DC) source is used to instead of distributed power supply to simplify analysis.

The main circuit of the system consists of a DC source, a three-phase voltage source inverter and ideal grid. According to the microgrid structure, some active and reactive loads are generally connected to the point of common coupling (PCC). R_g and L_g are line impedances; R_L, L and C are the resistance, filter inductor and capacitor of the LC filter, respectively; u_o and i_o are the output voltage and current of the inverter, respectively; i_c is the current of capacitor. The output powers are obtained by sampling u_o and i_o. They are used to generate the voltage reference signal in the VSG controller. Similar to most DG control methods, the voltage loop adopts quasi-PR controller to ensure tracking precision.

2.2 Power–frequency controller

The power–frequency controller of the VSG mainly simulates the rotor motion equation of SGs, which adopts the traditional second-order model of SGs in [22]:

$$\begin{cases} J\dfrac{\mathrm{d}\omega}{\mathrm{d}t} = T_\mathrm{m} - T_\mathrm{e} - T_d = \dfrac{P_\mathrm{m}}{\omega_0} - \dfrac{P_\mathrm{e}}{\omega_0} - D(\omega - \omega_\mathrm{g}) \\ \dfrac{\mathrm{d}\delta}{\mathrm{d}t} = \omega \end{cases} \tag{1}$$

where J is the rotational inertia, D is the damping torque, P_m is the mechanical power of SG, P_e is the electromagnetic power and ω and ω_g are the reference angular velocity of the VSG and grid synchronous angular velocity, respectively. Generally, ω_g can be replaced by grid reference angular velocity ω_0.

To simulate the primary frequency modulation of SGs, the governor is adopted in power–frequency controller, as shown in Fig. 1*b*. The governor expressed as (2) can be regarded as an active power and frequency droop control equation:

$$P_\mathrm{m} = P_\mathrm{ref} + k_\mathrm{p}(\omega_0 - \omega) \tag{2}$$

where P_ref is the active power reference. Let $K_\mathrm{d} = D + (k_\mathrm{p}/\omega_0)$, $\omega_\mathrm{g} = \omega_0$ and $\Delta\omega = \omega - \omega_0$, then (2) can be Laplace transformed as follows:

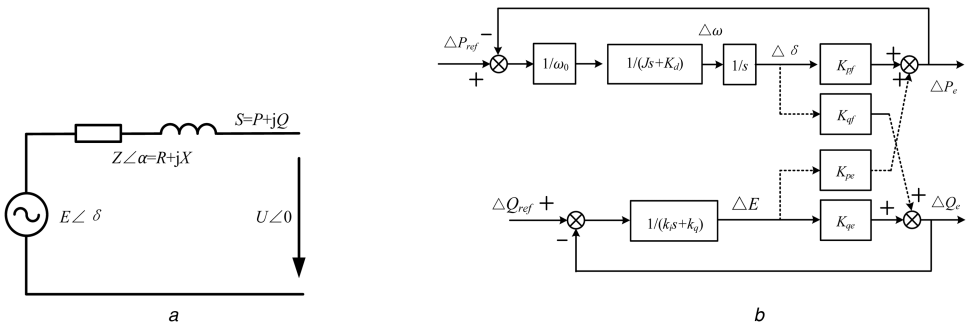

Fig. 2 *Simplified equivalent model*
(a) Equivalent model of a microgrid, ***(b)*** Small-signal equivalent model of VSG

$$\frac{P_{\text{ref}} + k_{\text{p}}(\omega_0 - \omega) - P_{\text{e}}}{\omega_0} - D(\omega - \omega_0) = Js\Delta\omega \tag{3}$$

Subsequently, a simplified equation can be derived as follows:

$$P_{\text{ref}} - P_{\text{e}} = (Js + K_d)\omega_0\Delta\omega \tag{4}$$

According to (4), both the damping factor and frequency modulation unit of the governor realise the function of damping power oscillation. The value of k_{p} is restricted by grid standards, and virtual inertia J causes the VSG to possess mechanical inertia, similar to those of SGs. The phase information of the reference voltage can be obtained from the power–frequency controller.

2.3 Structure of the excitation controller

Fig. 1*c* shows the structure of excitation controller including voltage and reactive power droop control and voltage regulator, which can be expressed as

$$E_{\text{m}} = \frac{1}{k_{\text{i}}}\int\left\{\left[k_q(U_n - U_{\text{o}}) + Q_{\text{ref}}\right] - Q_{\text{e}}\right\} + E_0 \tag{5}$$

where Q_{ref} is the reactive power reference, E_0 is the no-load voltage, U_n is the RMS of terminal voltage, k_q is the droop coefficient of voltage and reactive power and k_{i} is the integral coefficient. Voltage and reactive power droop control equation can make inverter realise primary voltage modulation. Amplitude value of reference voltage can be obtained from excitation controller. By synthesising the amplitude and phase information, the reference voltage e_{m} is generated as input of the voltage loop, which can be written as

$$\begin{cases} e_{\text{m}a} = \sqrt{2}E_{\text{m}}\sin\theta \\ e_{\text{m}b} = \sqrt{2}E_{\text{m}}\sin\left(\theta - \dfrac{2}{3}\pi\right) \\ e_{\text{m}c} = \sqrt{2}E_{\text{m}}\sin\left(\theta + \dfrac{2}{3}\pi\right) \end{cases} \tag{6}$$

2.4 Voltage control inner loop

In this article, the voltage loop adopts the widely used quasi-PR controller. Its transfer function can be written as

$$G_{\text{PR}}(s) = K_{\text{p}} + \frac{2K_{\text{r}}\omega_{\text{e}}s}{s^2 + 2\omega_{\text{e}}s + \omega_0^2} \tag{7}$$

where K_{p}, K_r and ω_{e} are the related control parameters, and ω_0 is the frequency benchmark value. In Fig. 1*d*, active damping inner loop based on capacity current feedback is used to restrain resonance and consequently prevent the oscillation generated by the disturbance of input side under light or no load condition. L and C represent the inductance and capacitance of the filter, respectively. The voltage loop transfer function expression can be expressed as follows, where $G_{\text{inv}}(s)$ is the transfer function of voltage and $Z_{\text{inv}}(s)$ represents the output impedance of the controller.

$$\begin{aligned} U_{\text{O}} &= \frac{G_{\text{PR}}(s)K_{\text{pwm}}}{LCs^2 + K_{ad}K_{\text{pwm}}Cs + G_{\text{PR}}(s)K_{\text{pwm}} + 1}E_{\text{m}} \\ &\quad - \frac{Ls}{LCs^2 + K_{ad}K_{\text{pwm}}Cs + G_{\text{PR}}(s)K_{\text{pwm}} + 1}I_{\text{O}} \\ &= G_{\text{inv}}(s)E_{\text{m}} - Z_{\text{inv}}(s)I_{\text{O}} \end{aligned} \tag{8}$$

3 Power coupling analysis

Fig. 2*a* shows the output power expressions of the inverter, with the line impedance considered. Subsequently, the active and reactive power flows injected into the power grid can be written as

$$\begin{aligned} P &= \frac{3U[E\cos(\alpha - \delta) - U\cos\alpha]}{Z} \\ Q &= \frac{3U[E\sin(\alpha - \delta) - U\sin\alpha]}{Z} \end{aligned} \tag{9}$$

where $E\angle\delta$ and $U\angle0$ are the output terminal voltage and the VPCC, respectively. R, X stands for the resistance and reactance of distributed line. The impedance of the line is $Z\angle\alpha = R + \text{j}X$.

In different voltage grades of power system, line impedance shows different characteristics. High-voltage overhead lines generally appears absolutely inductive, whereas low-voltage overhead lines appear resistive. Table 1 shows the output power expressions with different system impedance angles α. [23]

When $\alpha = 90°$, the active and reactive power can realise independent control. In this case, changes in frequency can only influence the output active power and changes in voltage amplitude may affect the output reactive power. However, as mentioned above, the power coupling mechanism in microgrids should be discussed because of its resistive or resistance–inductance environment.

Considering the output power deviation caused by disturbance ΔE and $\Delta\delta$ at quiescent point (E_s, δ_s), the following equations can be expressed after linearisation: (see (10)) where K_{pf}, K_{qf}, K_{pe} and

Table 1 Output power of inverter under different impedance

Impedance angle α	Inductive, $\alpha = 90°$	Resistive, $\alpha = 0°$	Resistance–inductance, $Z = R + \text{j}X$
active power	$\frac{3EU}{Z}\delta$	$\frac{3U(E - U\cos\delta)}{Z}$	$\frac{3EU}{Z}\cos(\alpha - \delta) - \frac{3U^2}{Z}\cos\alpha$
reactive power	$\frac{3U(E - U\cos\delta)}{Z}$	$\frac{-3EU}{Z}\delta$	$\frac{3EU}{Z}\sin(\alpha - \delta) - \frac{3U^2}{Z}\sin\alpha$

$$\begin{cases} \Delta P = \dfrac{3E_s U}{Z}\sin(\alpha-\delta_s)\Delta\delta + \dfrac{3U}{Z}\cos(\alpha-\delta_s)\Delta E = K_{pf}\Delta\delta + K_{pe}\Delta E \\ \Delta Q = \dfrac{-3E_s U}{Z}\cos(\alpha-\delta_s)\Delta\delta + \dfrac{3U}{Z}\sin(\alpha-\delta_s)\Delta E = K_{qf}\Delta\delta + K_{qe}\Delta E \end{cases} \tag{10}$$

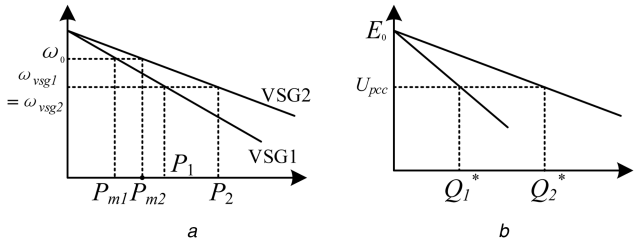

Fig. 3 *Droop unit of VSG*
(a) Principle of active power and frequency droop, ***(b)*** Principle of reactive power and VPCC droop

K_{qe} are used to denote the proportion gains of the corresponding variables. All of them can be calculated in a given system [14].

From (1), (4), (5) and (10), the small signal model of power loop can be deduced as shown in Fig. 2*b* [9].

According to (10) and Fig. 2*b*, $|K_{pe}|$ and $|K_{qf}|$ gradually increase with decreased impedance angle, which means that strong coupling exists between active and reactive power controls. This coupling may cause the appearance of a circumfluence in each loop and affect the stability of the system. Therefore, the power decoupling scheme for microgrid should be redesigned.

4 Power decoupling scheme for VSG

Each power decoupling method of a microgrid inverter presents advantages and disadvantages. Power decoupling for VSG has some new characteristics due to VSG's unique power loop circuit.

4.1 Active power and frequency independent control

Fig. 2*b* shows that the closed-loop transfer function expression of active power can be written as follows:

$$G_{\mathrm{p}} = \frac{\Delta P_{\mathrm{e}}}{\Delta P_{\mathrm{ref}}} = \frac{K_{pf}}{J\omega_0 s^2 + K_d\omega_0 s + K_{pf}} \tag{11}$$

According to (11), it is an I-type system [24]. Only if the control unit is stable, output active power and rotor frequency can track their reference signals accurately. Thus, VSG control strategy can cause the output side of the inverter to present 'sync' mechanism of SGs.

With the globalisation and transitivity of the frequency in a microgrid, namely, $\omega_{\mathrm{vsg}i} = \omega_{\mathrm{g}}$ ($i = 1, 2\ldots$), as shown in Fig. 3*a*, the output active power reference values of each VSG are all the same under the condition of same droop coefficients. Therefore, on the premise of system stability, the different output reactive powers of each VSG cannot affect their respective output active power, despite the mode (grid-connected or island) they are running in. In other words, VSG strategy can independently realise active power and frequency decoupling control. The physical significance is also definite. The frequencies of each inverter are clamped by a microgrid in grid-connected mode, and they are equal to network frequency in island mode. This feature causes the inverters to allocate the active power on the basis of droop coefficients.

4.2 Reactive power and voltage decoupling control

The coupling between reactive power and voltage is different from that in previous section. The output voltage of each micro-source should be consistent to achieve power independent control from the output voltage and reactive power droop equation in Fig. 1*c*. Nevertheless, as a result of the existence of line voltage drop, output voltages are not same when the output active powers of micro-sources change, which may affect the output reactive powers. Traditional decoupling control mainly focuses on compensating line voltage drop. Although its physical significance is explicit, the implementation process is complicated and requires complex design and calculation. Moreover, system stability is a limiting factor. In this paper, based on the decoupling principle of previous section, an independent variable can be obtained through introducing the voltage feedback of PCC, which is unaffected by the line voltage drop. In other words, as shown in Fig. 3*b*, VPCC can help inverters obtain the independent control of output reactive power [5].

However, different from the output voltage of inverter, the flexible geographical location of distributed generation renders VPCC difficult to obtain. Although communication is used in a microgrid to exchange message, the control principle of inverters is preferred to implement basic functions independently. Therefore, according to output voltage, current and line impedance, an improved structure with VPCC estimator for excitation controller shown in Fig. 4 is proposed. This scheme can be expressed as follows:

$$u_{\mathrm{pcc\_calculate}} = u_{\mathrm{o}} - R_{\mathrm{g}} i_{\mathrm{o}} - L_{\mathrm{g}}\frac{\mathrm{d}i_{\mathrm{o}}}{\mathrm{d}t} \tag{12}$$

In Fig. 4, R_{g} and L_{g} are the parameters of line impedance, $\omega_{\mathrm{c}}/(s + \omega_{\mathrm{c}})$ is the low-pass filter that suppresses high-frequency noises and k_{v} is the voltage adjustment coefficient. The VPCC can be obtained approximately by improving the excitation controller. Thus, the independent control of the output reactive power can be implemented, similar to previous section. This method essentially changes the impedance environment of the system and can be regarded as a deformation of virtual impedance. However, the influence of line impedance on output power can be almost counteracted with proposed method. Furthermore, reactive power sharing can be achieved by controlling the calculated VPCC to track its reference value, and this method is an improvement of the traditional virtual impedance decoupling method.

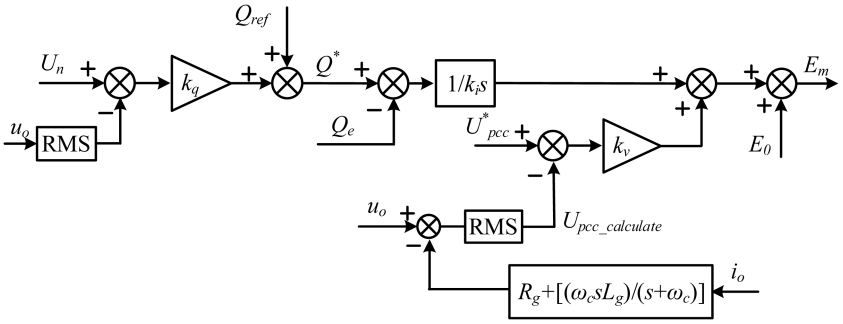

Fig. 4 *Improved excitation controller*

4.3 Stability analysis and parameter selection

The stability issues of the system can be divided into two categories. The first factor is the stability of the power loop, including the active power loop and reactive power loop. With the appropriate parameters, the power loop can exhibit good stability and dynamic performance at the double fundamental frequency [9]. The other factor focuses on the output current and voltage of the inverter at the non-fundamental frequency. The response of the system is the superposition of the responses at all frequency bands, and any instability in the response current may affect the entire system. In this section, the second factor of the stability issues is studied. According to Fig. 4 and (8), the transfer function between the feedback current and the output voltage can be written as follows:

$$Z_{\text{pcc}}(s) = \frac{\Delta u_{\text{o}}}{\Delta i_{\text{o}}} = \frac{k_{\text{v}} G_{\text{inv}}(s)(R_{\text{g}} + (\omega_{\text{c}} L_{\text{g}} s/(s+\omega_{\text{c}})))}{k_{\text{v}} G_{\text{inv}}(s) + 1} \tag{13}$$

Thus, the integrated impedance with line parameters can be derived as

$$Z(s) = Z_{\text{inv}}(s) + Z_{\text{pcc}}(s) + sL_{\text{g}} + R_{\text{g}} \tag{14}$$

As can be seen from (14), the integrated impedance of the inverter $Z(s)$ consists of three parts: inverter output impedance, equivalent VPCC estimator impedance and line impedance. From Fig. 2*a* and (8), the output current of the inverter can be written as

$$\Delta i_{\text{o}}(s) = \frac{\Delta E_{\text{m}}(s) G_{\text{inv}}(s) - \Delta U(s)}{Z(s)} \tag{15}$$

The numerator of (15) is stable when the voltage loop is correctly designed. Thus, the stability of the system admittance, $1/Z(s)$, should be analysed to ensure the stability of the entire system. According to the root-locus method, the system is stable if $1/Z(s)$ has no poles in the right-half s-plane [24]. The system admittance, $1/Z(s)$, can be expressed as

$$\frac{1}{Z(s)} = \frac{1}{Z_{\text{inv}}(s) + Z_{\text{pcc}}(s) + sL_{\text{g}} + R_{\text{g}}} = \frac{Y_{\text{num}}(s)}{Y_{\text{den}}(s)} \tag{16}$$

In this study, let $Y_{\text{den}}(s) = 0$. Subsequently, the root locus of this characteristic equation can be plotted by changing the voltage adjustment coefficient, k_{v}. The system parameters are shown in Table 2.

In Fig. 5*a*, according to the viewpoint of automatic control theory [24], all branches of the root locus are located in the left-half s-plane, which means that the system is always stable regardless of the change in k_{v}. There are three dipoles in the root-locus plot. Thus, their influence on the system performance can be ignored. Accordingly, the fifth-order system can be simplified into a second-order system. The other two dominant poles moving along the direction of the arrows are a pair of conjugate complex roots. In accordance with the design principle of the optimal second-order system, we select $k_{\text{v}} = 55.8$ to achieve a damping ratio of 0.707 for the system. Consequently, the Bode diagram of the system admittance can be generated. In Fig. 5*b*, at the fundamental frequency (314 rad/s), the system admittance is $112\angle -0.27°$ S, which indicates that the system impedance presents inductive, and its amplitude is so small that can be neglected. Furthermore, the open-loop cut-off frequency of the system admittance is 2.72×10^5 rad/s, and the corresponding phase margin is 66°. These results show that the selected parameters comply with the design requirement.

Table 2 Parameter settings for the VSG algorithm

Parameters	Values	Parameters	Values
L	2 mH	V_{dc}	800 V
C	500 μF	K_{p}	4
R_{L}	0.05 Ω	K_r	100
R_{g}	0.5 Ω	δ_{s}	0.07
X_{g}	0.83 Ω	ω_{e}	6.5
ω_0	314 rad/s	U^*_{pcc}	220 V
E_s	235.7 V	ω_{c}	5000 rad/s
J	0.45		

4.4 Selection of droop coefficient

The previous section states that the selection of proportionality coefficient k_{p} and reactive droop coefficient k_q are dependent on grid standards. According to GB/T12325-2008 and GB/T15945-2008, the deviation of three-phase power supply voltage under 20 kV is ±7% of nominal voltage and the fluctuation range of grid frequency is ±0.5 Hz. This paper defines that the change of 100% active power (15 kW) corresponds to the change of 1% grid frequency, while the change of 100% reactive power (3 kVar) corresponds to the 7% change in the grid nominal voltage. Consequently, the following equation is obtained:

$$k_{\text{p}} = \frac{\Delta P_{\max}}{\Delta \omega} \simeq 4777, \quad k_q = \frac{\Delta Q_{\max}}{\Delta U_{\max}} \simeq 195 \tag{17}$$

5 Simulation and experimental analysis

5.1 Simulation analysis

When the microgrid is running in grid-connected mode, the grid can support the frequency and voltage of the microgrid. Then the fluctuation of load cannot result in the change of frequency or voltage, which is the primary cause of power coupling. So, all of following simulation verification are based on islanded microgrid. Furthermore, it needs to be stressed that all of output power waveforms are measured at PCC to show the decoupling effect more clearly and visualised.

The proposed power decoupling scheme has been verified in MATLAB/Simulink. In Fig. 6*a*, a microgrid platform with two 30 kVA DGs, 30 kW/6 kVar public load Z_{Ld1}, 10 kW active fluctuating load Z_{Ld2} and 2 kVar reactive fluctuating load Z_{Ld} is employed. According to above analysis, the circuit breaker QF is always open. With the same power rating, the two DGs should share the load equally. The corresponding parameters of the DGs are listed in Table 2. To get a more realistic case, the line impedance of two DGs is different: $Z_{\text{L1}} = 0.5 + \text{j}0.83\ \Omega$, $Z_{\text{L2}} = 0.7 + \text{j}0.41\ \Omega$.

5.1.1 Performance of the VSG control: The performance of VSG control method is illustrated in Fig. 7. The power reference values are $P_{\text{ref1}} = P_{\text{ref2}} = 15$ kW, $Q_{\text{ref1}} = Q_{\text{ref2}} = 3$ kVar. The control parameters are $K_{\text{dvsg1}} = 20$, $K_{\text{dvsg2}} = 20$, $k_{q1} = k_{q2} = 195$, $k_{\text{i1}} = 10$, $k_{\text{i2}} = 5$. The switch S_1 and S_2 are closed at 0.4 s and opened at 0.8 s simultaneously. In Fig. 7*a*, the active power sharing is always accurate. However, due to the existence of line impedance, there are obvious errors in reactive power sharing. On the other hand, as can be seen in Fig. 7*b*, decreasing frequency of the system and VPCC are associated with increased active power and reactive power, which shows the droop characters of the output power. However, the increased power cannot match the fluctuating loads, which means the coupling between active and reactive power is existed.

5.1.2 Verification of proposed power decoupling method: In this part, the power reference values are $P_{\text{ref1}} = P_{\text{ref2}} = 15$ kW and $Q_{\text{ref1}} = Q_{\text{ref2}} = 3$ kVar. The control parameters are $K_{\text{dvsg1}} = 20$, $K_{\text{dvsg2}} = 40$, $k_{q1} = k_{q2} = 0.005$, $k_{\text{i1}} = k_{\text{i2}} = 6$, $k_{\text{v1}} = k_{\text{v2}} = 56$. Different K_ds are used to vary the output active power of two inverters. The time duration of simulation is 1 s. Two VSGs run in islanded mode, and switch S_1 is closed at 0.5 s. Fig. 8 shows a comparison results with and without decoupling control.

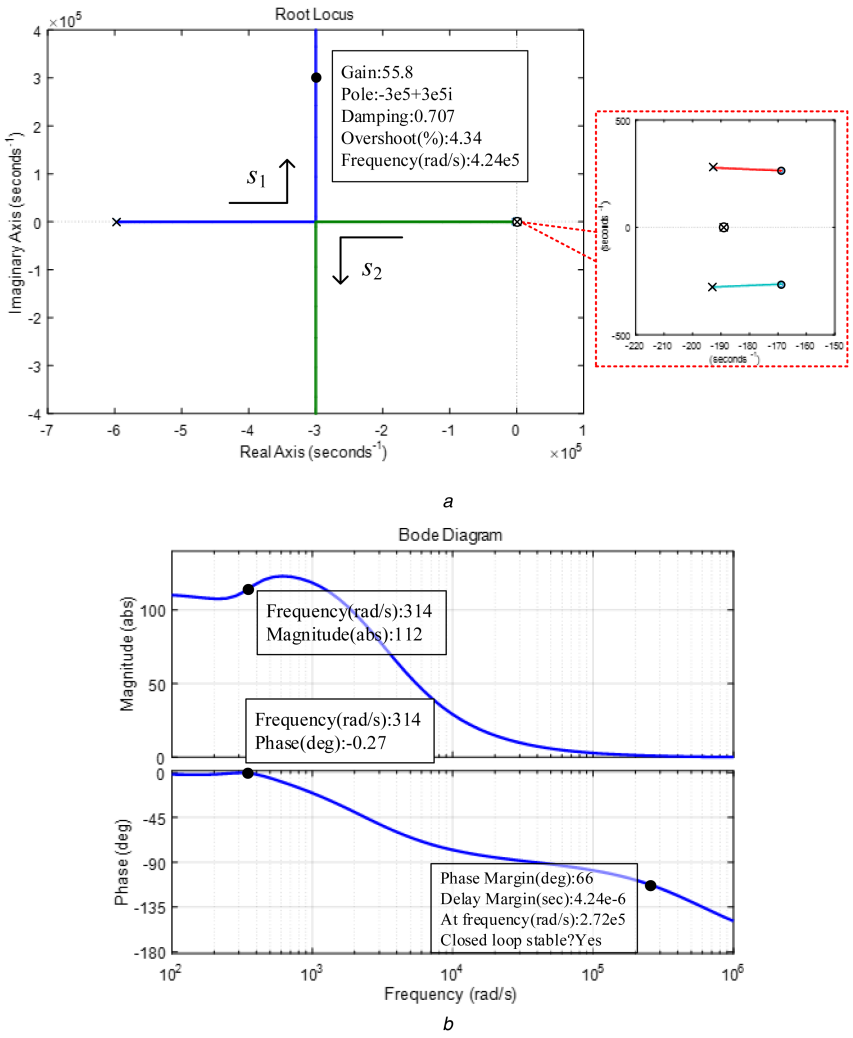

Fig. 5 *Stability criterion of the system admittance*

(a) Root-locus plot of the system admittance, ***(b)*** Bode diagram of the system admittance

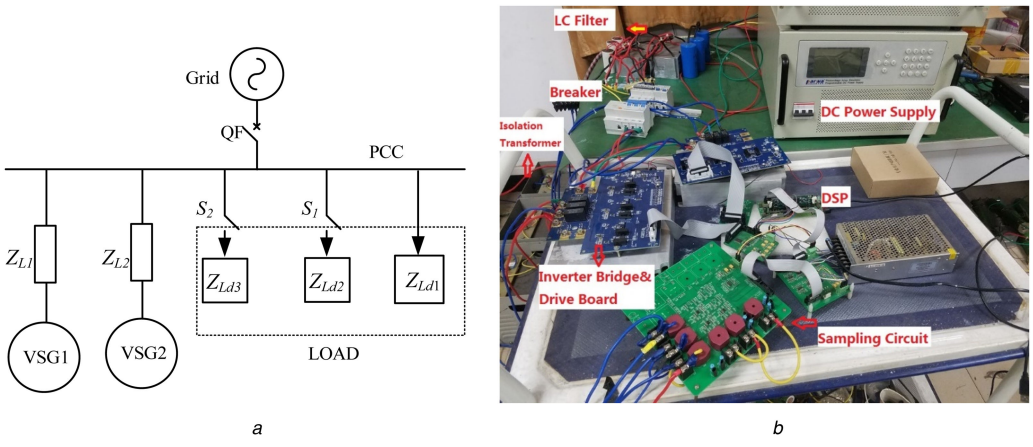

Fig. 6 *Microgrid structure with two VSGs*

(a) The microgrid simulation diagram, ***(b)*** Microgrid experiment platform

The results shown in Fig. 8*a* show that, under the disturbance of fluctuating active load, different output active power affects the reactive power sharing. Furthermore, the total reactive power decreases by increasing the active power. Fig. 8*b* shows that although the active power of two inverters is changed, the output reactive power of two VSGs still tracks their reference values, which verifies that VSG with VPCC estimator can obtain good effect of power decoupling.

Then, the influence of fluctuating reactive load is verified. The time duration of simulation is 1 s and switch S_2 is closed at 0.5 s. The power reference values are $P_{\text{ref1}} = P_{\text{ref2}} = 15$ kW, $Q_{\text{ref1}} = Q_{\text{ref2}} = 3$ kVar. The control parameters are $K_{\text{dvsg1}} = 20$, $K_{\text{dvsg2}} = 20$, $k_{q1} = k_{q2} = 195$, $k_{\text{i1}} = 10$, $k_{\text{i2}} = 5$, $k_{\text{v1}} = k_{\text{v2}} = 56$. Different k_{i}s are used to vary the output reactive power of two inverters. Fig. 9 shows the comparison results with and without decoupling control.

The results in Fig. 9*a* show that, before integrating the decoupling control, the disturbance of a fluctuating reactive load may result in a decrease in the output active power. However, owing to the strong disturbance-resisting capability of the second-order system and the small coupling component based on (10), the difference in the output reactive power does not result in the degradation of the quality of the active power sharing. Fig. 9*b*

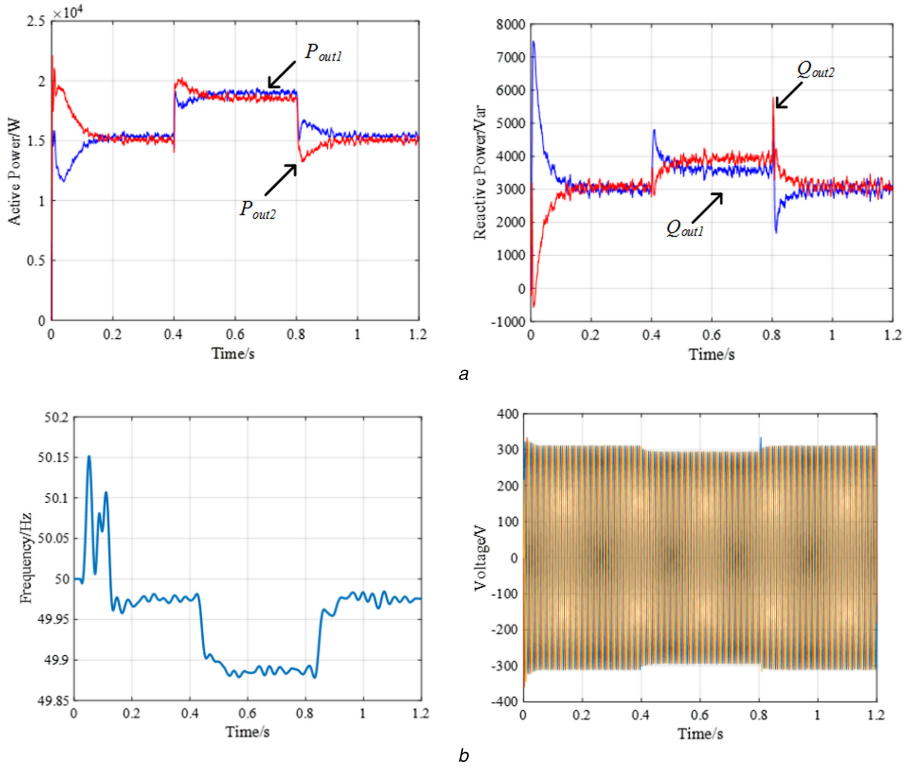

Fig. 7 *Simulated performance of the VSG control method*

(a) The output active and reactive power waveforms, ***(b)*** The frequency and VPCC of the system

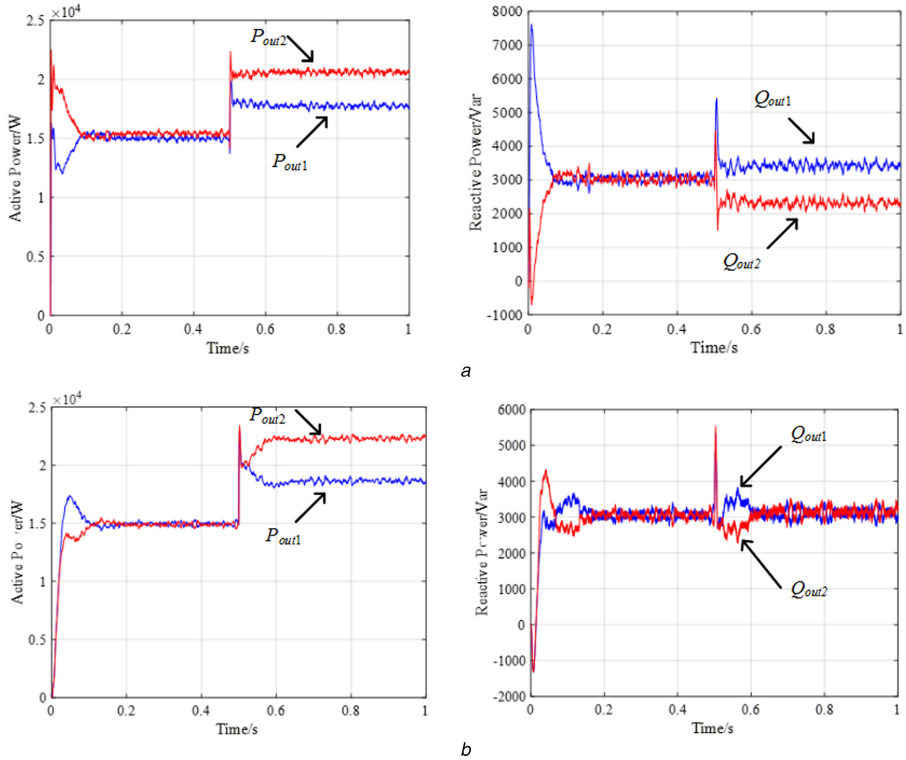

Fig. 8 *Comparison of the results with and without decoupling control*

(a) Waveforms of active and reactive power without decoupling control, ***(b)*** Waveforms of active and reactive power with decoupling control

verifies that the change in the output reactive power cannot affect the output active power.

5.2 Experimental analysis

This paper uses an existing microgrid experimental platform for the experimental verification, as shown in Fig. 6*b*. The platform has same topological structure and parameters with the simulation part. The DC power supply adopts AGP1030. The main circuit of the inverter adopts the integration module CCS050M12CM2 from CREE. The driving circuit for the switch tube uses the integration module CGD15FB45P. The main controller of the system adopts the DSP chip (TMS320F28335) from TI Company. MS/RS30 programmable power supply of AMETEK is used to simulate the grid frequency fluctuation and deviation of voltage amplitude.

Both two VSGs run in grid-connected mode and VSG1 adopts improved scheme and VSG2 uses traditional method. Their power reference values are $P_{ref1} = P_{ref2} = 10$ kW and $Q_{ref1} = Q_{ref2} = 5$

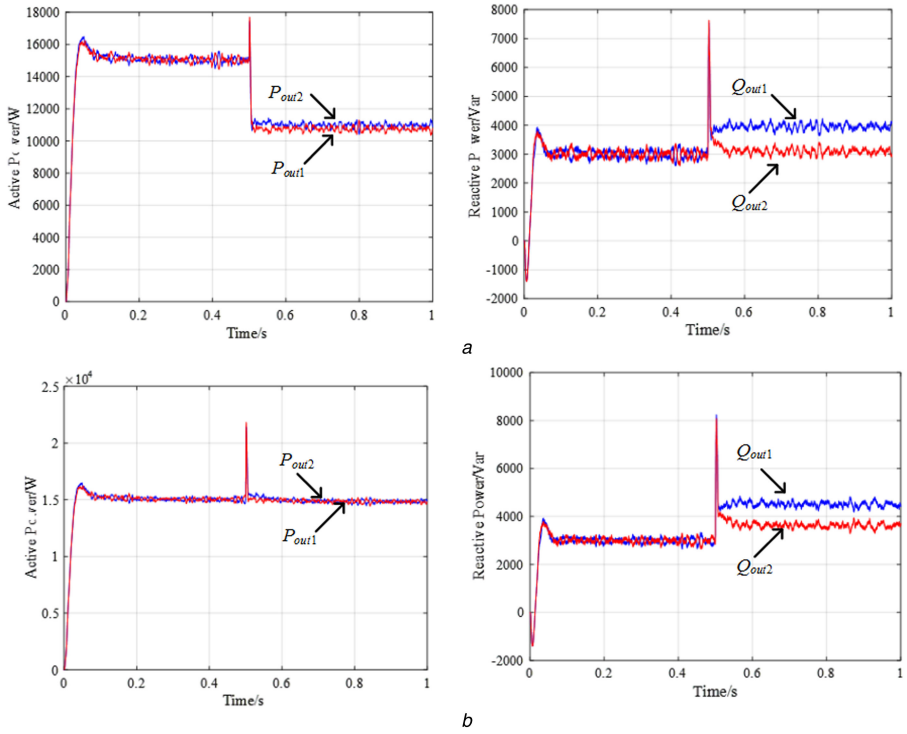

Fig. 9 *Comparison results with and without decoupling control*

(a) Waveforms of active and reactive power without decoupling control, ***(b)*** Waveforms of active and reactive power with decoupling control

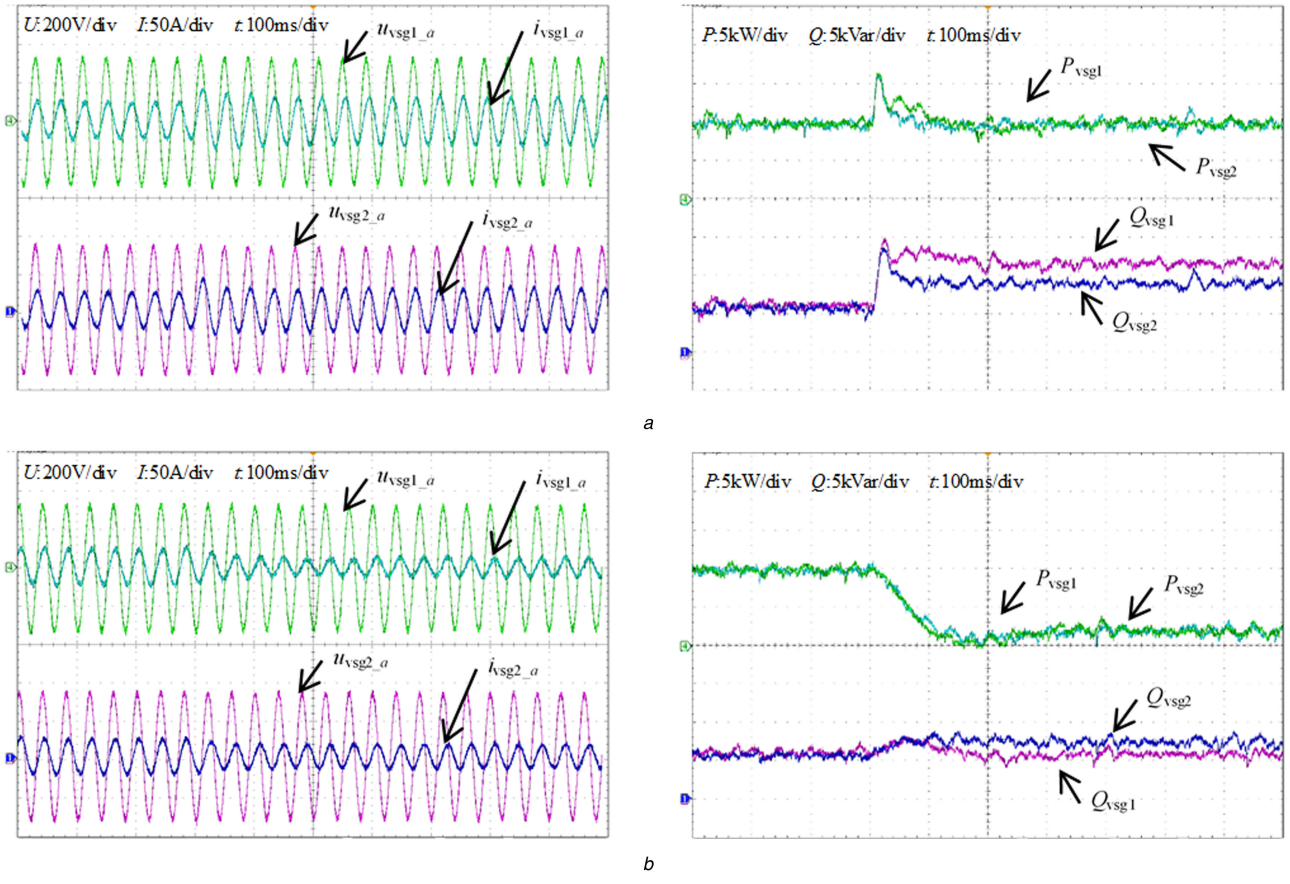

Fig. 10 *Output response waveforms under an abrupt change*

(a) Output response waveforms under abrupt voltage change, ***(b)*** Output response waveforms under abrupt frequency change

kVar. The control parameters are $K_{dvsg1} = 20$, $K_{dvsg2} = 20$, $k_{q1} = k_{q2} = 0.005$, $k_{i1} = k_{i2} = 6$, $k_{v1} = 56$. Fig. 10 shows the response waveforms after the grid voltage decreases by 0.05 p.u., and frequency increases 0.2 Hz suddenly.

Fig. 10*a* illustrates that VSG control scheme can realise primary voltage regulation, namely, changes output reactive power of inverter against voltage deviation of grid side. Its voltage-regulating ability depends on reactive power droop coefficient k_q. The difference in the reactive power of two VSGs after decreasing grid voltage by 0.05 p.u. is generated by changes in output current. This difference can be eliminated through adjusting the reactive power droop coefficient k_q. Obviously, the output active power

tracks its reference value and is unaffected by the change in reactive power.

Fig. 10*b* shows that VSG can realise primary frequency regulation function. According to (4), the output active power decreases $K_d\omega_0\Delta\omega$ (about 7800 W) when frequency increases by 0.2 Hz. Subsequently, the output reactive power of VSG1 can still track its reference value, whereas VSG2 cannot. Corresponding output current of VSG1 decreases more than that of VSG2 to ensure the same output active power.

6 Conclusion

An improved power decoupling scheme for VSG is proposed in this article. Active power and reactive power independent controls are discussed by analysing the power coupling mechanism of VSG in medium- and low-voltage microgrids. Only when the system is stable can VSG realise active power and frequency independent control. In addition, an improved excitation controller for reactive power independent control is presented. Compared with traditional virtual impedance method, the new strategy requires no complex design and calculation and can enable better power decoupling effect. The stability analysis and parameter selection are also provided. Consequently, the proposed decoupling strategy is a significant supplement for VSG in microgrids. Finally, simulation and experimental results are presented to verify the effectiveness of the proposed method.

7 Acknowledgments

This work was supported by the National Natural Science Foundation of China (Grant no. 51477021) and the '111' State Innovation & Talent Recruitment Base (B08036).

8 References

[1] Lasseter, R.H.: 'Microgrids'. IEEE Power Engineering Society Winter Meeting, New York, 2002

[2] Azmy, A.M., Erlich, I.: 'Impact of distributed generation on the stability of electrical of electrical power system'. Power Engineering Society General Meeting, San Francisco, 2005

[3] Aktarujjaman, M., Haque, M.E., Muttaqi, K.M., *et al.*: 'Control stabilisation of multiple distributed generation'. Power Engineering Conf., Australia, 2007

[4] Lu, L.-Y., Chu, C.-C.: 'Consensus-based secondary frequency and voltage droop control of virtual synchronous generators for isolated AC micro-grids', *IEEE J. Emerging Sel. Topics Circuits Syst.*, 2015, **5**, (3), pp. 443–455

[5] Zhong, Q.-C., Nguyen, P.-L., Ma, Z.: 'Self-synchronized synchronverters: inverters without a dedicated synchronization unit', *IEEE Trans. Power Electron.*, 2014, **29**, (2), pp. 617–630

[6] Driesen, J., Visscher, K.: 'Virtual synchronous generators'. IEEE Power Energy Soc. Gen. Meeting, USA, 2008

[7] Shintai, T., Miura, Y., Ise, T.: 'Oscillation damping of a distributed generator using a virtual synchronous generator', *IEEE Trans. Power Deliv.*, 2014, **29**, (2), pp. 668–676

[8] Liu, J., Miura, Y., Ise, T.: 'Comparison of dynamic characteristics between virtual synchronous generator and droop control in inverter-based distributed generators', *IEEE Trans. Power Electron.*, 2016, **31**, (5), pp. 3600–3611

[9] Heng, W., Xinbo, R., Dongsheng, Y.: 'Small-signal modeling and parameters design for virtual synchronous generators', *IEEE Trans. Ind. Electron.*, 2016, **63**, (7), pp. 4292–4303

[10] Zhang, L., Harnefors, L., Nee, H.-P.: 'Power-synchronization control of grid-connected voltage-source converters', *IEEE Trans. Power Syst.*, 2010, **25**, (2), pp. 809–820

[11] Ashabani, M., Mohamed, Y.A.R.I.: 'Integrating VSCs to weak grids by nonlinear power damping controller with self-synchronization capability', *IEEE Trans. Power Syst.*, 2014, **29**, (2), pp. 805–814

[12] Brabandere, K.D., Bolsens, B., Keybus, J.V.D., *et al.*: 'A voltage and frequency droop control method for parallel inverters', *IEEE Trans. Power Electron.*, 2007, **22**, (4), pp. 1107–1115

[13] Yun, W.L., Chingnan, K.: 'An accurate power control strategy for power-electronics-interfaced distributed generation units operating in a low-voltage multi-bus microgrid', *IEEE Trans. Power Electron.*, 2009, **24**, (12), pp. 2977–2988

[14] Yan, X., Zhang, Y.: 'Power coupling analysis of inverters based on relative gain method and decoupling control based on feedforward compensation'. International Conf. on Renewable Power Generation (RPG 2015), Beijing, 2015

[15] Li, P., Yang, S., Yin, Z.: 'Voltage stabilization and decoupling droop control method for microgrid based on RGA', *Proc. CSEE*, 2015, **35**, (5), pp. 1041–1050 (in Chinese)

[16] Rowe, C.N., Summers, T.J., Betz, R.E., *et al.*: 'Arctan power-frequency droop for improved microgrid stability', *IEEE Trans. Power Electron.*, 2013, **28**, (8), pp. 3747–3759

[17] Wu, T., Liu, Z., Liu, J.: 'A unified virtual power decoupling method for droop-controlled parallel inverters in microgrids', *IEEE Trans. Power Electron.*, 2016, **31**, (8), pp. 5587–5603

[18] Zhu, Y., Zhuo, F., Wang, F., *et al.*: 'A wireless load sharing strategy for islanded microgrid based on feeder current sensing', *IEEE Trans. Power Electron.*, 2015, **30**, (12), pp. 6706–6719

[19] Mahmood, H., Michaelson, D., Jiang, J.: 'Accurate reactive power sharing in an islanded microgrid using adaptive virtual impedances', *IEEE Trans. Power Electron.*, 2015, **30**, (3), pp. 1605–1617

[20] He, J., Li, Y.W., Blaabjerg, F.: 'An enhanced islanding microgrid reactive power, imbalance power, and harmonic power sharing scheme', *IEEE Trans. Power Electron.*, 2015, **30**, (6), pp. 3389–3401

[21] Zhang, P., Zhao, H., Cai, H., *et al.*: 'Power decoupling strategy based on 'virtual negative resistor' for inverters in low-voltage microgrids', *IET Power Electron.*, 2016, **9**, (5), pp. 1037–1044

[22] Bergen, A.R., Vittal, V.: '*Power systems analysis*' (Pearson Hall Press, 1999, 2nd edn.), pp. 258–259

[23] Vandoorn, T.L., Meersman, B., Degroote, L., *et al.*: 'A control strategy for islanded microgrids with DC-link voltage control', *IEEE Trans. Power Deliv.*, 2011, **26**, (2), pp. 703–713

[24] Franklin, G.F.: '*Feedback control of dynamic systems*' (Pearson Education Limited Press, 2014, 7th edn.)